Performance of the Cosmic Hot Interstellar Plasma Spectrometer

Martin M. Sirk[a], Geoffrey Gaines[b], Ellen R. Taylor[a], Michael Sholl[a], William Marchant[a], Richelieu Hemphill[a], Randy A. Kimble[c], Timothy Sasseen[d], Mario Marckwordt[a], and William Donakowski[a]

[a]Space Sciences Laboratory, University of California, Berkeley CA, USA
[b]Gaines Systems, Inc
[c]Goddard Space Flight Center, Greenbelt MD, USA
[d]Dept. of Physics, University of California, Santa Barbara CA, USA

ABSTRACT

The Cosmic Hot Interstellar Plasma Spectrometer (CHIPS), successfully launched on 2003 January 12, provides astronomers with an observatory dedicated to observation of the hot interstellar medium in the extreme ultraviolet. We describe here the optical and photometric performance of the spectrograph based on calibrations of the individual components, end-to-end vacuum tests, and in-orbit observations of the Moon.

Keywords: EUV astronomy

1. INTRODUCTION

The Cosmic Hot Interstellar Plasma Explorer (CHIPS) is a NASA UNEX mission devoted to diffuse background spectroscopy in the EUV passband 90 to 260 Å. NASA launched CHIPS from Vandenberg AFB on 2003 January 12 as a secondary payload on a Delta II rocket into a circular polar orbit with an inclination of 94° and an altitude of 590 km.

The 3-axis stabilized satellite consists of a 35 kg spacecraft built by SpaceDev, Inc. and a 25 kg science instrument provided by the University of California. The integrated assembly is about 100 by 100 by 30 cm (about the size of a large suitcase). The spectrograph consists of microchannel plate detector mounted at the focus of six identical varied line space (VLS) diffraction gratings which are illuminated by six identical slit mechanisms. The science objectives of CHIPS are outlined in Hurwitz *et al.*[1] and the opto-mechanical design of the instrument detailed in Sholl *et al.*.[2]

The CHIPS mission is being carried out in two phases. The opening of the detector door, opening of the slit mechanisms, and ramping up the detector high voltage to full operational levels comprised the first phase. The second phase is devoted to mapping as much of the sky as feasible. About 300 pointings are required to tile the celestial sphere with the 4° by 26° field of view of CHIPS.

2. INSTRUMENT DESCRIPTION

2.1. Optical Bench

Unlike traditional spectrographs the CHIPS design does not employ a telescope to gather light. For each channel diffuse EUV radiation enters a slit and intercepts a cylindrically surfaced VLS grating at a mean graze angle of 14°. The first internal or "inside" order is then directed towards a microchannel plate detector. Since a cylindrical grating surface greatly reduces off-axis optical aberrations (relative to a spherical surface), channel replication is possible. CHIPS employs six identical gratings which, when properly co-aligned, show smaller off-axis aberrations than a single grating of equivalent area. To minimize the effects of thermal flexure between

Further author information: (Send correspondence to M.M.S.)
M.M.S.: E-mail: sirk@ssl.berkeley.edu

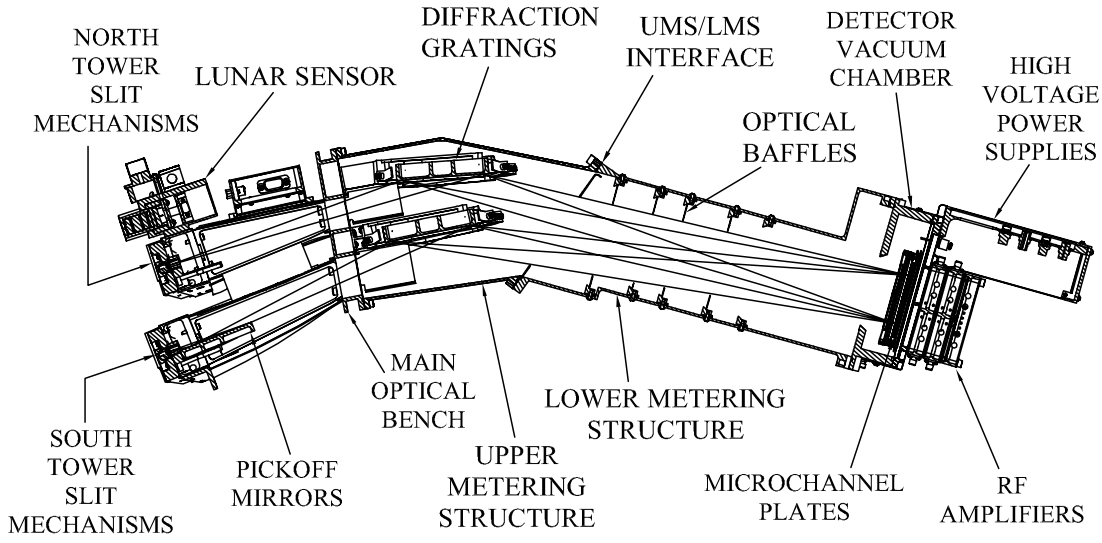

Figure 1. Profile view of CHIPS showing two channels.

the six channels, the gratings and slit mechanisms are cantilevered on opposite sides of the main optical bench (Figure 1). Flexure displacements are then primarily parallel to the light paths.

Each grating was replicated from a mechanically ruled VLS submaster onto a weight relieved Zerodur cylindrical blank (R=147.8 cm) and overcoated with rhodium to enhance reflectivity in the EUV. Each slit mechanism contains a slotted cylinder which can be rotated into one of three positions; closed, wide, and narrow. The narrow slit is 7 cm by 0.025 cm and provides a resolution of $\lambda/FWHM \approx 120$. The resolution of the wide slit (7 cm by 0.1 cm) is about 1/3 that of the narrow, but with 4 times the throughput.

2.2. Detector and Filters

The six co-aligned gratings focus a single image of the slits onto microchannel plate (MCP) detector. The design is that of the GALEX[3] mission and consists of a "Z" stack of 75 mm diameter MCPs with 12 μm pores oriented 13° from the focal plane normal. The glass and nichrome top plate surface is overcoated with NaBr to create a photocathode with enhanced sensitivity in the EUV and an active area 65 mm in diameter.

Each photoelectron produces an electron cascade in the MCP which is read out by a cross delay line anode. The total charge and centroid of the charge cloud are determined by onboard electronics. High and low charge events are excluded by onboard thresholding. Each event is telemetered to the ground at an (X,Y) precision of 4096 by 4096. A detector spatial resolution of 86 μm (3.5 px, or $\approx$ 0.35Å) was determined from pinhole mask data. These data were also used to quantify detector distortions.

A filter frame that holds four vacuum deposited thin film ($\sim$ 1000Å thick) filters is mounted 8.8 mm above the detector face. The filter transmissions are chosen to maximize the signal to noise ratio in the three different passbands by suppressing higher diffracted orders as well as longer wavelength scattered and stray light. Figure 2 shows the filter locations, their constituent materials, and the wavelength scale of the spectrograph. A complete analysis of the CHIPS detector is given by Marckwordt and Gaines.[4]

3. CALIBRATIONS

Because CHIPS is a diffuse (non-imaging) spectrograph, the Moon proved to be the only in-orbit calibration source (point sources, including the EUV bright white dwarf HZ 43, are not detectable). Therefore, considerable attention was paid to ground calibrations. The simplicity of the CHIPS instrument inspired the following calibration strategy:

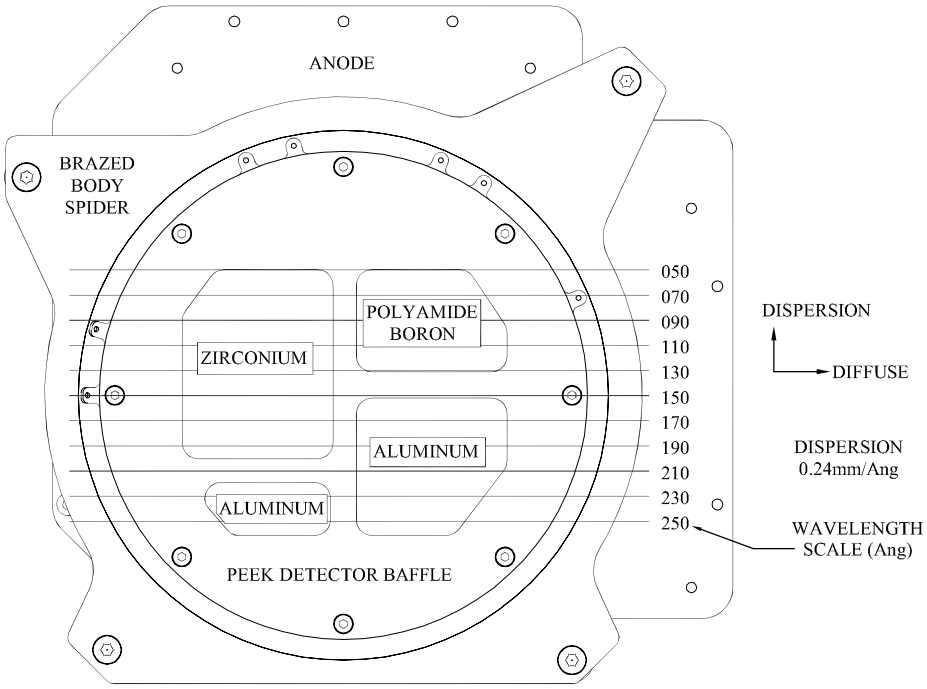

Figure 2. Detector filter frame.

1. Characterize the performance of the CHIPS components (gratings, pickoff mirrors, and filters) individually with continuous EUV radiation, and the detector quantum detection efficiency (QDE) at a set of discrete wavelengths.

2. On the integrated instrument, determine absolute throughput, the wavelength scale, and the out-of-band response to scattered/stray light at a set of discrete wavelengths.

3. On-orbit, use Moon pointings to verify focus, wavelength scale and throughput.

Comparing the measured performance of the complete instrument to the predicted performance based on the component measurements provided powerful cross-checking. We discuss each step in the next subsections.

3.1. Components

All calibrations were conducted at the University of California, Berkeley. The diffraction gratings, pickoff mirrors, and filters were tested with synchrotron radiation at Advanced Light Source (ALS) of the Lawrence Berkeley Laboratory. Supplemental tests on these components were performed at the Space Sciences Laboratory (SSL) with discrete emission line sources. The detector QDE was also measured at SSL at discrete wavelengths. The component efficiencies are presented as Figure 3. The six gratings and three pickoff mirrors showed very consistent efficiencies and are thus presented as averages.

3.2. Instrument

The complete spectrograph was tested in the large tank of the SSL vacuum calibration facility. A diverging beam of EUV radiation located 4 m from the entrance apertures and a translation table were used to simulate on- and off-axis illumination. Different emission line sources were used in tests to verify alignment, determine wavelength scale, throughput, and response to stray and scattered out-of-band light.

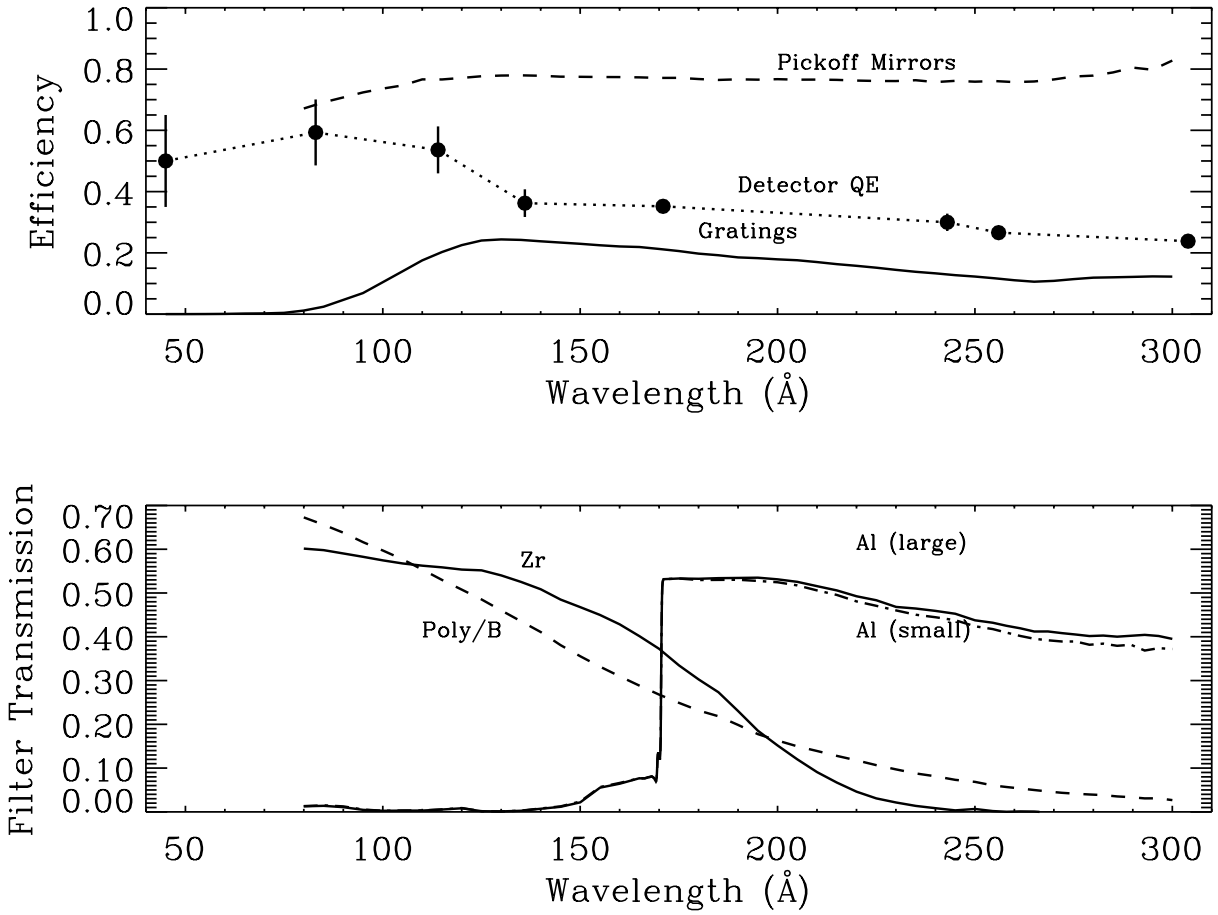

Figure 3. Component efficiencies (top) and filter transmissions (bottom).

3.3. Moon Observations

Each month CHIPS is pointed at the full moon for 10 to 20 ks to observe reflected Solar emission spectra. About 8 significant Fe lines are suitable to verify pointing accuracy, and to check for wavelength shifts. Any major changes in instrument throughput should be measurable and the absolute throughput may be roughly estimated. We further discuss the Moon observations in section 6.

4. OPTICAL PERFORMANCE

4.1. Line Response Function and Wavelength Scale

A hollow Al/Mg cathode gas discharge source provided EUV radiation at multiple wavelengths suitable for resolution tests and wavelength calibration. After achieving final alignment (by translating and rotating the six slit mechanisms by fractions of a mm) spectra were obtained in each channel both on- and off-axis. Figure 4 shows the combined on- and off-axis spectra of all six channels which provides a good approximation of a diffuse source. Double Gaussians were fit to the identified lines to determine centroids and line widths. Spectra from two additional sources (Be 114.0Å and He 256.3Å) were combined with those of Figure 4 for the wavelength scale determination. A second order polynomial fit to the wavelength *vs.* detector X position showed an RMS residual of 0.05Å. The spectrograph dispersion, wavelength scale residuals, and the measured spectral resolution $\lambda/FWHM$ and raytrace model prediction are shown as Figure 5.

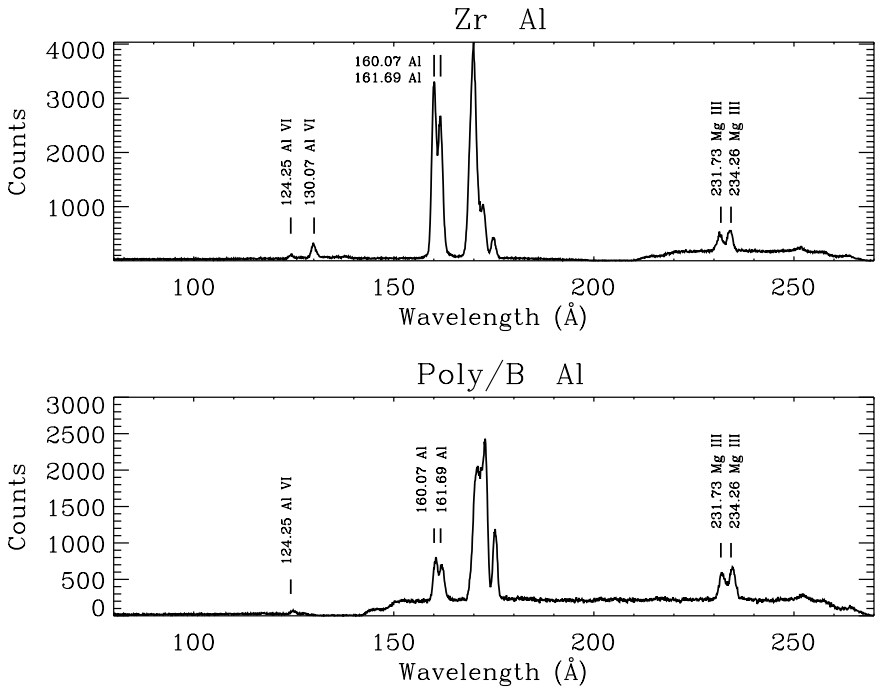

Figure 4. Al/Mg emission line spectrum for the Zr/Al filters (top), and the Poly/B filters (bottom). Lines used for wavelength scale and resolution determinations are identified.

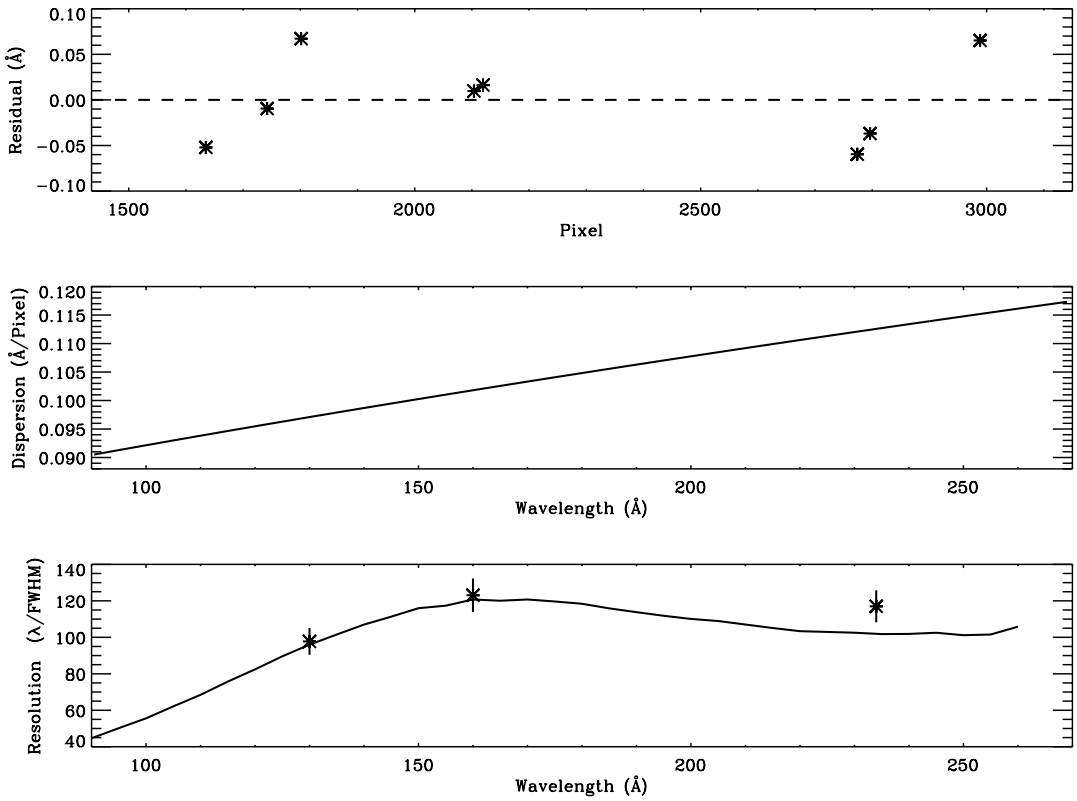

Figure 5. Residuals from polynomial fit (top), spectrograph dispersion (middle), and spectral resolution (bottom). Measured lines widths are shown as symbols, and the predicted ray trace model resolution shown as a solid line.

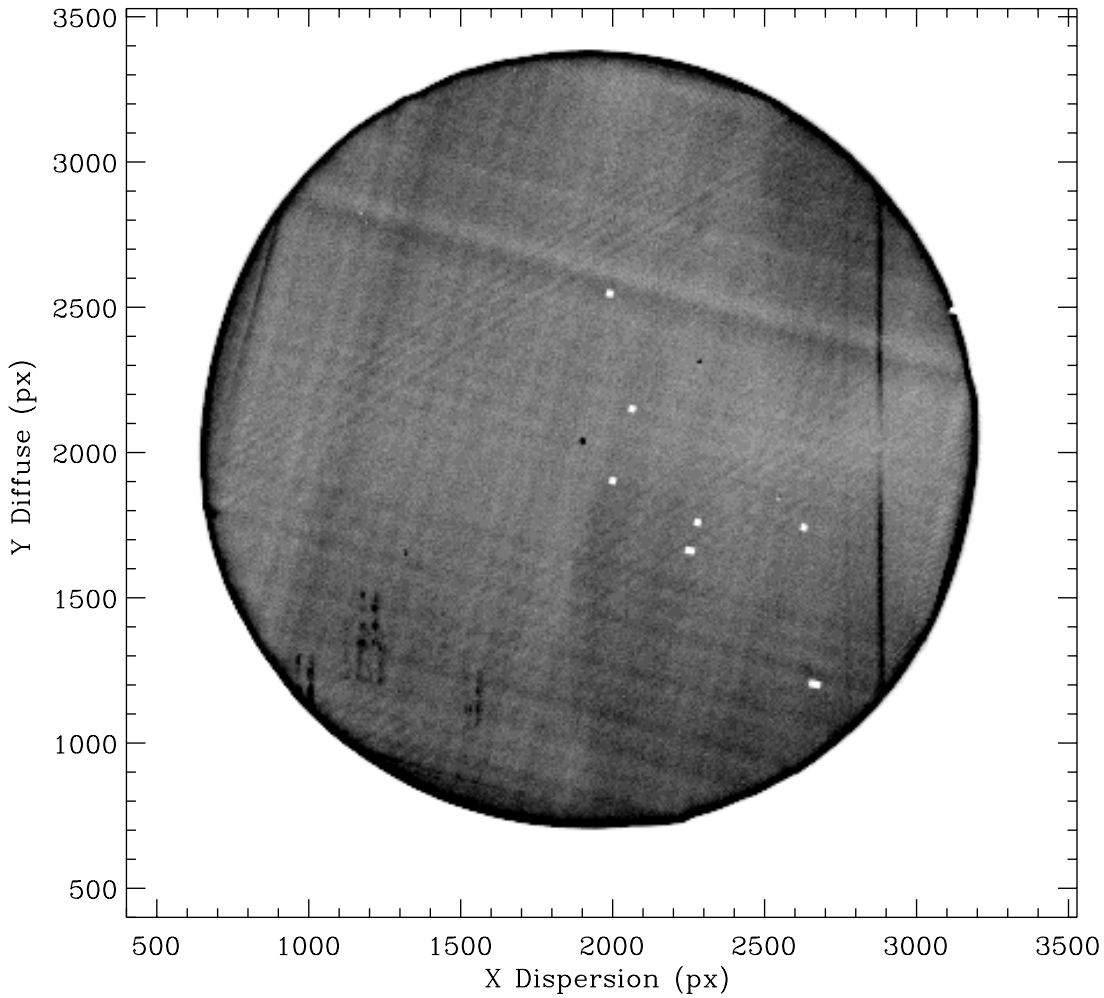

Figure 6. Detector image of daytime data. The two Al panels appear to the right, the Zr top left, and Poly/B lower left. The He 256Å and He 243Å lines are the vertical lines at right. The stray light features appear at lower left. Wavelength increases to the right (opposite that of Figure 2.) Small white regions are the locations of excluded hotspots.

4.2. Scattered and Stray Light

Great effort was expended to minimize the effects of unwanted light. Baffles are located in the slit mechanisms, on the main optical bench, on the grating mounts, and the lower metering structure (Figure 1). All internal metal surfaces are bead blasted to reduce reflection efficiency. Except for the entrance apertures themselves, the spectrograph is light-tight. The primary source of out-of-band signal is geocoronal/interplanetary line emission (He 304Å, He 584Å, and H 1216Å) that scatters off the gratings directly onto the detector. The scattering levels were quantified during ground calibrations by illuminating the entrance apertures with each of the above lines at a known intensity and comparing the observed detector countrates in each filter panel to the dark countrate. Assuming daytime intensities of 6, 440, and 22,000 Rayleighs for He 304, He 584 and H 1216, respectively, yielded a predicted background daytime rate of 0.053 (ct s^{-1} cm^{-2}) and a nighttime rate of 0.005 (ct s^{-1} cm^{-2}). We compare these predicted rates to the actual on-orbit rates in section 6.

Grating scattering measurements were also performed at the component level both in- and out-of-band. At 90Å and 170Å the in-band values are 5.52×10^{-4} $arcmin^{-1}$ and 2.60×10^{-4} $arcmin^{-1}$, respectively.[5] Observations obtained with the complete spectrograph with a Be 114Å source yielded a scattering value $\sim 5 \times 10^{-4} arcmin^{-1}$.

The flight data show several stray light features in the Poly/B filter panel during daytime observations. These are manifest as seven pairs of vertical streaks ~0.6 cm tall. Each artifact consists of two parallel features,

strongly suggesting that stray light, passing through both slits, is being imaged. Figure 6 is a detector image of daytime data and shows scattered He 584Å light in the Al filter panels, and stray light features in the Poly/B panel. The strength of the features does not correlate with measured He 256Å line strength, nor the scattering levels of He 584Å seen in the Al panels. The most likely cause is H 1216Å light that is diffracted off the 5 mm wide visible ruling patches[2] at the end of the gratings closest to the detector. Raytrace modeling shows that the features are not caused by a direct path from the entrance aperture to the gratings, but rather by an indirect path involving at least one internal reflection, or potentially illumination of a grating by light from a "wrong" entrance slit pair.

5. EFFECTIVE AREAS AND FIELD OF VIEW

5.1. Effective Areas

For each channel, the effective area for a given filter type is the product of the grating efficiency, the pickoff mirror efficiency (if employed), the detector QDE, the filter transmission (which are all functions of wavelength, see Fig. 3), and the geometrical area of the slit. Adding the six channels results in the final effective area curves. Figure 7 shows the curves based on the component measurements for the narrow slits. The wide slits have greater effective areas by a factor of 4. Throughput measurements of the completed spectrograph for each filter type (plotted as dots in Figure 7) are 15% less on average than the predicted values based on the components. Thus, our best estimate of pre-flight effective area is probably 15% less than the curves shown in Figure 7.

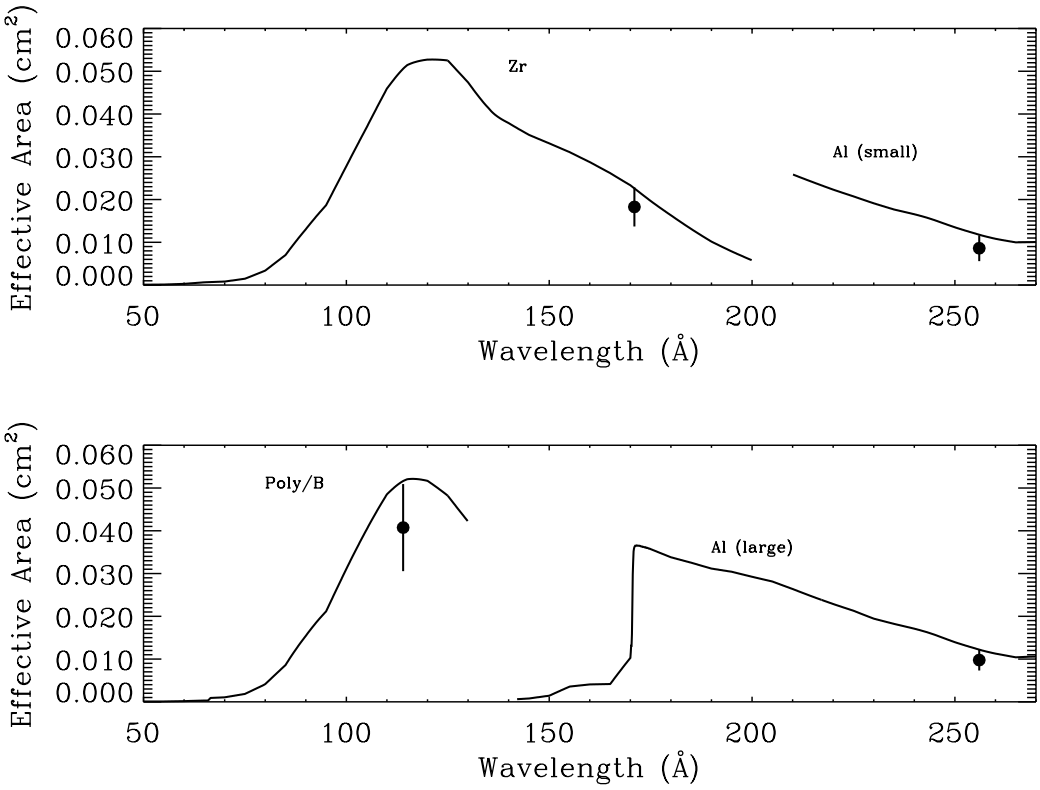

Figure 7. Effective area curves for the four filter panels based on component continuum measurements (lines) and measured values of spectrograph throughput at discrete wavelengths (dots).

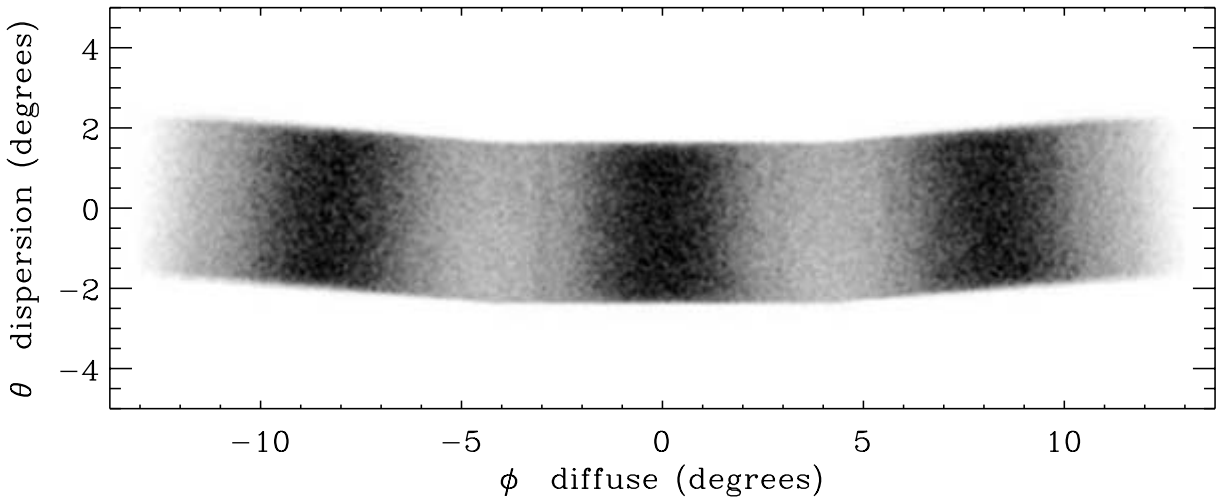

Figure 8. Vignetting of CHIPS field of view. Black is zero vignetting, white represents complete vignetting. The integral of this image yields $\Omega = 0.00531$ str.

5.2. Vignetting of the Field of View

Because CHIPS is a diffuse (non-imaging) spectrograph, the ultimate sensitivity is the product of the effective area and the solid angle Ω subtended by the field of view. The true Ω is determined by raytrace models that input rays from all possible angles corresponding to the maximum field of view. The ratio of the number of rays that strike the detector to the input number of rays, times the maximum Ω, is then the true Ω. This value is 0.00531 str for the center of the passband λ =170Å. Figure 8 depicts the relative sensitivity of the CHIPS field of view. Because the detector is a circle, Ω varies with wavelength and drops to 73% and 56% of its maximum value at 70Å and 260Å, respectively.

6. IN–FLIGHT PERFORMANCE

Each orbit, the CHIPS satellite passes through the electron belts at high magnetic latitude. Chips also passes periodically through the SAA. Total detector countrates in these regions may exceed 2000 ct s^{-1}. Outside of these high particle regions countrates typically vary from 10 to 100 ct s^{-1}. We chose an upper threshold of 70 ct s^{-1} (which corresponds to 2.2 ct s^{-1} cm^{-2}) for science analysis. By taking advantage of the different MCP pulse height distributions between photons and particles, the particle background was reduced by $\sim 40\%$. Table 1 lists the typical day and night background levels for the three filter passbands after thresholding. The nighttime background level is quite low ($\sim$ 11 ct s^{-1} over the entire detector). Scattered light increases the daytime background level by up to 0.18 ct s^{-1} cm^{-2} which is about 3.5 times higher than predicted from ground calibrations.

Table 1. CHIPS flight background levels (ct s^{-1} cm^{-2}).

	Al	Zr	Poly/B
Day	0.56	0.43	0.48
Night	0.38	0.35	0.36

Analysis of spectral features from the Moon pointings showed a constant shift in wavelength scale of about 1.1Å (about 0.275 mm). The spectral resolution as determined from the He 256Å line and a few of the brightest Fe lines shows no change from prelaunch values. The observed CHIPS full moon countrates are consistent with

the preflight calibration response curve. With the exception of the stray light features in the Poly/B filter, the spectrometer performs as designed.

ACKNOWLEDGMENTS

This work is supported by the Office of Space Sciences, National Aeronautics and Space Administration, under Grant No. NAG5-5219.

REFERENCES

1. M. Hurwitz, "Status of the cosmic hot interstellar plasma spectrometer (CHIPS) university-class explorer mission," *Proc. SPIE*, 2002.
2. M. Sholl, W. Donakowski, M. M. Sirk, T. Clauss, M. Lampton, J. Edelstein, and M. Hurwitz, "Opto-mechanical design of the cosmic hot interstellar plasma spectrometer (CHIPS)," *Proc. SPIE*, 2002.
3. O. H. W. Siegmund, P. Jelinsky, J. Stock, J. Hull, D. Doliber, J. Zaninovich, A. S. Tremsin, and K. Kromer, "High resolution cross delay line detectors for the GALEX mission," in *EUV, X-Ray, and Gamma-Ray Instrumentation for Astronomy*, *Proc. SPIE 3765*, pp. 429–440, 1999.
4. M. R. Marckwordt, G. A. Gaines, J. Edelstein, R. Hemphill, J. Hoberman, J. Hull, M. Hurwitz, M. Lampton, W. Marchant, K. McKee, T. P. Sasseen, M. Sholl, O. Siegmund, M. Sirk, D. Stone, and E. R. Taylor, "EUV detector of the Cosmic Hot Interstellar Plasma Spectrometer (CHIPS)," in *UV/EUV and Visible Space Instrumentation for Astronomy II*, *Proc. SPIE*, 2003.
5. R. Hemphill, "Os atomic O protection by an Ir overcoat for increased EUV grating efficiency," *Applied Optics* **Sept.**, 2003.